

ANALYSIS OF LOCAL IMAGE STATISTICS TO IMPROVE MEDICAL IMAGE SEGMENTATION

A Thesis Proposal
Presented to
The Academic Faculty

by

Shawn M. Lankton

In Partial Fulfillment
of the Requirements for the Degree
Doctor of Philosophy in the
School of Electrical and Computer Engineering

Georgia Institute of Technology
January 21, 2009

ANALYSIS OF LOCAL IMAGE STATISTICS TO IMPROVE MEDICAL IMAGE SEGMENTATION

Approved by:

Professor Anthony Yezzi, Committee Chair
School of Electrical and Computer
Engineering
Georgia Institute of Technology

Professor Allen Tannenbaum, Advisor
School of Electrical and Computer
Engineering
Georgia Institute of Technology

Professor Jeff Shamma
School of Electrical and Computer
Engineering
Georgia Institute of Technology

Professor X
School of Electrical and Computer
Engineering
Georgia Institute of Technology

Date Approved: Not Yet Approved

TABLE OF CONTENTS

SUMMARY	iv
I JUSTIFICATION OF THE RESEARCH TOPIC	1
1.1 Introduction	1
1.2 The Problem Under Investigation	2
1.2.1 Active Contours in Segmentation	3
1.2.2 Localized Methods	4
II PRELIMINARY RESEARCH	6
2.1 Localization Framework	6
2.2 Various Internal Energy Measures	9
2.2.1 Uniform Modeling (UM) Energy	10
2.2.2 Mean Separation (MS) Energy	11
2.2.3 Histogram Separation (HS) Energy	12
2.3 Localized Segmentation Results	13
2.4 Fiber Bundle Segmentation	16
2.4.1 Background and Relevance	17
2.4.2 Localized Statistics on Tensor Data	19
2.4.3 Experiments on Cingulum Bundle Segmentation	21
III THE PROPOSED RESEARCH	23
3.1 Summary of Work Completed	23
3.2 Work Remaining to Be Done	24
3.2.1 Development of Theory and Implementation	24
3.2.2 Additional Applications	25
3.2.3 Validation and Preparation of Publications	26
3.3 Facilities Needed	26
APPENDIX A DERIVATION OF CURVATURE FLOW	27
REFERENCES	29

SUMMARY

Computer vision attempts to approximate the abilities of human vision artificially on computers and is used extensively in surveillance, industrial automation, robotics, military tracking, and medical image processing just to name a few applications. The proposed research is in the field of image segmentation, a subset of computer vision that attempts to separate an image into logical parts that correspond to objects or regions of interest.

The objective of the proposed research is to explore and improve the use of localized image information for image segmentation and consider potential applications to medical image processing. Specifically, a framework has been created that naturally allows local – rather than global – image statistics to drive image segmentation. Experiments have shown that localized contours are capable of segmenting objects with heterogeneous feature profiles that would be difficult to capture correctly using existing global methods.

In the first medical application considered, localized segmentation was used to produce accurate segmentations of neural fiber bundles in the brain. Additional medical applications will include the segmentation of vessel walls in coronary blood vessels to facilitate the automatic detection of soft plaque. Finally, to complete the research, the theory and implementation of the proposed framework will be developed further and the work will be validated and prepared for publication. All of this is expected to be completed by August 2009.

CHAPTER I

JUSTIFICATION OF THE RESEARCH TOPIC

In this chapter, the field of computer vision is introduced and special treatment is given to image segmentation and active contour models specifically. Next, the problems addressed by this research are given and explained. Finally, relevant work in the literature that motivates and supports the proposed research is discussed. Much of this chapter is based on [20].

1.1 Introduction

Computer vision emerged in the 1970s with the goal of approximating the abilities of human vision artificially on computers [13]. Vision is perhaps the most important sense used by humans to understand the world around them. While the human vision system remains far more complex than man-made approximations, research in this field has resulted in huge leaps in technological capabilities. Computer vision is now used extensively in surveillance, industrial automation, robotics, military tracking, and medical image processing just to name a few applications [14].

Within computer vision, one can consider three high-level operations: image acquisition, image understanding, and assignment of meaning. The first operation deals with the sensor that produces the image and the processing that needs to be performed in order for the image to contain usable data. The image understanding operation, which includes the proposed research, deals with segmenting the image into salient objects and tracking movement. Finally, the assignment of meaning bridges the gap between computer vision and artificial intelligence. The third operation will be outside the scope of this research. In practice meaning is often assigned by the human user or is inherent in the application.



(a) AIRPLANE



(b) HUG

Figure 1: (a) The AIRPLANE image is simple to segment because the foreground and background are very different. (b) The HUG image is much harder due to the complex image patterns and intensity distributions.

Specifically, the focus of the proposed research is image segmentation. Breaking an image into parts is often a first step in understanding it. Accurate segmentations are necessary for information about the size, shape, orientation, and interaction of objects to be determined. While our biological vision system performs this task very simply, doing so automatically with computers has proven to be very complicated. Research over the past thirty years has made tremendous progress, and there still remains much to be done.

1.2 *The Problem Under Investigation*

The problem under investigation is that of separating an image into regions that correspond to unique objects of interest within the scene. This is particularly challenging when the objects have complex appearances that are not easily modeled or distinguished from other objects or the background. Addressing this specific case is the problem considered here. This situation occurs to some extent in all but the simplest images. In order to successfully segment these challenging images using existing methods, one must create intricate models that describe the object's appearance exactly. However, this can become difficult as the complexity of the image increases. Consider the images in Figure 1. The AIRPLANE image is simple to segment because the object (the airplane) can be easily distinguished from the background by

the brightness of the image pixels. However, in the HUG image showing two prairie dogs, the animals and the background have similar intensities that are not consistent or easily distinguishable. As a result, the HUG image is difficult to segment using existing methods.

The specific aim of this research is to construct a simple, tractable, mathematical framework that improves segmentations on complex images and then study the potential applications to real-life segmentation problems in medical imaging.

1.2.1 Active Contours in Segmentation

Active contours are one class of methods that has been used for image segmentation [5]. The basic idea is to use a deformable contour (or deformable surface for 3D segmentations) that starts from a rough initialization and is moved until it eventually settles on the boundary of the object of interest. The movement of the contour is guided by assigning an energy based on the location of the contour and the underlying image data. This energy is then minimized by moving the contour via gradient descent until an optimum is obtained.

The first type of active contour segmentation models were edge-based models that utilized image gradients in order to identify object boundaries, e.g., [17, 8]. This type of segmentation assumed that object boundaries would be located at areas that showed rapid intensity changes. While this assumption is often true, rapid intensity changes also occur where no object boundaries exist. In edge-based models, no consideration was given to regions inside or outside the contour; only pixels very close to the interface were examined. This type of highly localized image information was adequate in some situations, but was found to be very sensitive to image noise and highly dependent on initial curve placement.

More recently, work in active contours has been focused on region-based flows inspired by the region-competition work of Zhu and Yuille [54]. These approaches

model the foreground and background regions statistically and find an energy optimum where the model best fits the image. Some of the most well-known and widely used region-based active contour models assume the various image regions to be of constant intensity [9, 52, 42, 53]. More advanced techniques attempt to model regions by known distributions, intensity histograms, texture maps, or structure tensors [43, 18, 11, 27].

There are many advantages of region-based approaches when compared to edge-based methods including robustness against initial curve placement and insensitivity to image noise. However, techniques that attempt to model regions using global statistics are usually not ideal for segmenting heterogeneous objects. In cases where the object to be segmented cannot be easily distinguished in terms of global statistics, region-based active contours may lead to erroneous segmentations. Heterogeneous objects frequently occur in natural and medical imagery. To accurately segment these objects, a new class of active contour energies should be considered which utilizes local information, but also incorporates the benefits of region-based techniques.

1.2.2 Localized Methods

There have been several methods in the literature which are relevant to the proposed work. Paragios and Deriche [36] presented a method in which edge-based energies and region-based energies were explicitly summed to create a joint energy which was then minimized. In [48, 49], Sum and Cheung take a similar approach and minimize the sum of a global region-based energy and a local energy based on image contrast. The idea of incorporating localized statistics into a variational framework begins with the work of Brox and Cremers [6] who show that segmenting with local means is a first order approximation of the popular piecewise smooth simplification [31] of the Mumford-Shah functional [32]. This focus on the piecewise smooth model is also presented in several related works as described here.

Li *et al.* [23] analyze the localized energy of Brox and Cremers and compare it to the piecewise smooth model in much more detail. However, there is no explicit analysis of the appropriate scale on which to localize [24]. Piovano *et al.* [40] focus on fast implementations employing convolutions that can be used to compute localized statistics quickly, and hence yield results similar to piecewise-smooth segmentation in a much more efficient manner. The work of An *et al.* [1] also notes the efficiency of localized approaches versus full piecewise smooth estimation. That work goes on to introduce a way in which localizations at two different scales can be combined to allow sensitivity to both coarse and fine image features. This recent attention focuses almost exclusively on the problem of approximating the piecewise smooth segmentation model and fails to address the broader benefits that localization of region-based energies can bring.

CHAPTER II

PRELIMINARY RESEARCH

In this chapter, a novel framework is presented that can be used to localize any region-based energy in a fully variational way. The significant improvement of localization within this framework is that objects which have heterogeneous statistics can be successfully segmented with localized energies when corresponding global energies fail. Using the framework, three localized energies are derived. The first, presented in Section 2.2.1, is similar to the energies presented in the prior work mentioned in Section 1.2.2. Two additional region-based segmentation energies and their localized counterparts are formulated in Sections 2.2.2 and 2.2.3. Experiments showing the improved performance of the localized segmentation techniques are then given. Finally, an application to the segmentation of brain structures is described and preliminary experiments are shown. Much of this chapter is based on [20, 21].

2.1 Localization Framework

In this section, the local region-based framework for guiding active contours is described. Within this framework, segmentations are not based on global region models. Instead, the foreground and background are described in terms of smaller local regions, thereby removing the assumption that foreground and background regions can be uniquely represented with global statistics.

Analysis of local regions leads to the construction of a family of local energies at each point along the curve. In order to optimize these local energies, each point is considered separately, and that point moves to minimize the energy computed in its own local region. To compute these local energies, local neighborhoods are split into local interior and local exterior by the evolving curve. The energy optimization is

then performed by fitting a model to each local region.

Let I denote a given image defined on the domain Ω , and let C be a closed contour represented as the zero level set of a signed distance function ϕ , i.e., $C = \{x|\phi(x) = 0\}$ [33, 34]. The interior of C is specified by the following approximation of the smoothed Heaviside function:

$$\mathcal{H}\phi(x) = \begin{cases} 1 & \phi(x) < -\epsilon \\ 0 & \phi(x) > \epsilon \\ \frac{1}{2}\left\{1 + \frac{\phi}{\epsilon} + \frac{1}{\pi}\sin\left(\frac{\pi\phi(x)}{\epsilon}\right)\right\} & \text{otherwise} \end{cases} \quad (1)$$

Similarly, the exterior of C is defined as $(1 - \mathcal{H}\phi(x))$. To specify the area just around the curve, the derivative of $\mathcal{H}\phi(x)$ will be used. This is a smoothed version of the Dirac delta:

$$\delta\phi(x) = \begin{cases} 1 & \phi(x) = 0 \\ 0 & |\phi(x)| < \epsilon \\ \frac{1}{2\epsilon}\left\{1 + \cos\left(\frac{\pi\phi(x)}{\epsilon}\right)\right\} & \text{otherwise} \end{cases} \quad (2)$$

A second spatial variable y is now introduced. Here, x and y will indicate independent spatial variables each representing a single point in Ω . Using this notation, a characteristic function $\mathcal{B}(x, y)$ is introduced in terms of a radius parameter r :

$$\mathcal{B}(x, y) = \begin{cases} 1 & \|x - y\| < r \\ 0 & \text{otherwise} \end{cases} \quad (3)$$

This characteristic function $\mathcal{B}(x, y)$ is used to mask local regions. This function will be 1 when the point y is within a ball of radius r centered at x , and 0 otherwise. The interaction of $\mathcal{B}(x, y)$ with the interior and exterior regions is illustrated in Figure 2. Using $\mathcal{B}(x, y)$, an energy functional is defined in terms of a generic force function, F . This energy is given as follows:

$$E(\phi) = \int_{\Omega_x} \delta\phi(x) \int_{\Omega_y} \mathcal{B}(x, y) \cdot F(I(y), \phi(y)) dy dx. \quad (4)$$

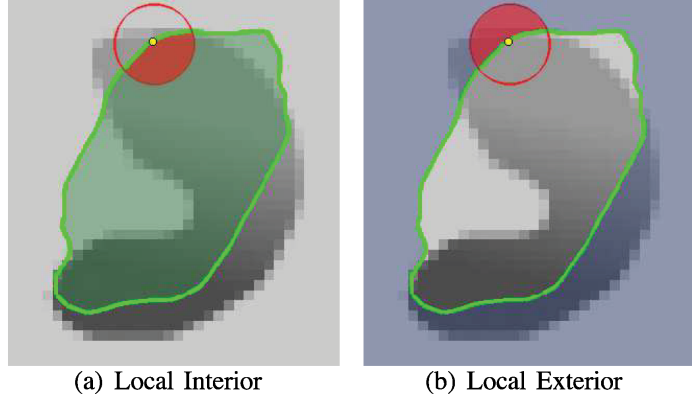


Figure 2: A ball is considered at each point along the contour. This ball is split by the contour into local interior and local exterior regions. In both images, the point x is represented by the small dot. The $\mathcal{B}(x, y)$ neighborhood is represented by the larger red circle. In (a) the local interior is the shaded part of the circle and in (b) the shaded part of the circle indicates the local exterior.

The function, F is a generic internal energy measure used to represent local adherence to a given model at each point along the contour. In Section 2.2, several possible candidates for F are examined and it is shown how any region-based energy can be modified and rewritten as an F to be included in this framework.

In computing E , only contributions from the points near the contour are considered. By ignoring inhomogeneity that may arise far away, this method has the ability to capture a much broader range of objects. In Equation (4) multiplication by the Dirac function, $\delta\phi(x)$ in the outer integral over x ensures this property. Note that this term ensures that the curve will not change topology by spontaneously developing new contours, although it still allows for contours to split and merge.

For every point x selected by $\delta\phi(x)$, $\mathcal{B}(x, y)$ is used as a mask to ensure that F operates only on local image information about x . Thus, the total contribution of the first term of the energy is the sum of F values for every $\mathcal{B}(x, y)$ neighborhood along the zero level set.

Finally, in order to keep the curve smooth, a regularization term is added as is commonly done. Penalization of the arclength of the curve is weighted by a parameter

λ . The final energy is given as follows:

$$E(\phi) = \int_{\Omega_x} \delta\phi(x) \int_{\Omega_y} \mathcal{B}(x, y) \cdot F(I(y), \phi(y)) dy dx + \lambda \int_{\Omega_x} \delta\phi(x) \|\nabla\phi(x)\| dx. \quad (5)$$

Taking the first variation of this energy with respect to ϕ , the following evolution equation is obtained (see Appendix A):

$$\frac{\partial\phi}{\partial t}(x) = \delta\phi(x) \int_{\Omega_y} \mathcal{B}(x, y) \cdot \nabla_{\phi(y)} F(I(y), \phi(y)) dy + \lambda \delta\phi(x) \operatorname{div} \left(\frac{\nabla\phi(x)}{|\nabla\phi(x)|} \right). \quad (6)$$

Notice that the only restriction on the internal energy, F is that its first variation with respect to ϕ can be computed. This ensures that nearly all region-based segmentation energies can be put into this framework.

2.2 Various Internal Energy Measures

Having formulated the framework in terms of a generic internal energy measure F , three specific energies are now introduced that can be inserted: the *uniform modeling energy*, the *means separation energy*, and the *histogram separation energy*. These energies are presented as examples of how any energy can be improved by localization, and no claim is made that one energy out performs the others in all cases. In this section, each global energy is briefly described, an intuitive description of its behavior is given, and then it is shown how it can be incorporated into the generic framework described above.

Two well known techniques [9, 53] make use of global mean intensities of the interior and exterior regions denoted as u and v respectively:

$$u = \frac{\int_{\Omega_y} \mathcal{H}\phi(y) \cdot I(y) dy}{\int_{\Omega_y} \cdot \mathcal{H}\phi(y) dy} \quad (7)$$

$$v = \frac{\int_{\Omega_y} (1 - \mathcal{H}\phi(y)) \cdot I(y) dy}{\int_{\Omega_y} \cdot (1 - \mathcal{H}\phi(y)) dy}. \quad (8)$$

In Sections 2.2.1 and 2.2.2, internal energy functions are discussed that rely on local mean intensities to separate regions. These sections use localized equivalents of

u and v defined in terms of the $\mathcal{B}(x, y)$ function. The localized versions of the means, u_x and v_x ,

$$u_x = \frac{\int_{\Omega_y} \mathcal{B}(x, y) \cdot \mathcal{H}\phi(y) \cdot I(y) dy}{\int_{\Omega_y} \mathcal{B}(x, y) \cdot \mathcal{H}\phi(y) dy} \quad (9)$$

$$v_x = \frac{\int_{\Omega_y} \mathcal{B}(x, y) \cdot (1 - \mathcal{H}\phi(y)) \cdot I(y) dy}{\int_{\Omega_y} \mathcal{B}(x, y) \cdot (1 - \mathcal{H}\phi(y)) dy} \quad (10)$$

represent the intensity means in the interior and exterior of the contour localized by $\mathcal{B}(x, y)$ at a point x . These localized statistics are needed to determine local energies at each point along the curve.

2.2.1 Uniform Modeling (UM) Energy

A well-known example of an energy that uses a constant intensity model energy is the Chan-Vese energy [9] referred to here as the *uniform modeling energy*:

$$E_{\text{UM}} = \int_{\Omega_y} \mathcal{H}\phi(y)(I(y) - u)^2 + (1 - \mathcal{H}\phi(y))(I(y) - v)^2 dy. \quad (11)$$

This energy models the foreground and background as constant intensities represented by their means, u and v . The corresponding internal energy function F is formed by replacing global means u and v by their local equivalents from Equations (23) and (24) as follows:

$$F_{\text{UM}} = \mathcal{H}\phi(y)(I(y) - u_x)^2 + (1 - \mathcal{H}\phi(y))(I(y) - v_x)^2. \quad (12)$$

This F can be substituted directly into Equation (5) to form a completely localized energy. In order to obtain the evolution equation for ϕ , the derivative of F is taken with respect to $\phi(y)$. The derivative can be written immediately as

$$\nabla_{\phi(y)} F_{\text{UM}} = \delta\phi(y) ((I(y) - u_x)^2 - (I(y) - v_x)^2). \quad (13)$$

By inserting this into Equation (6), the curvature flow for the localized version of

the uniform modeling energy is obtained:

$$\begin{aligned}\frac{\partial \phi}{\partial t}(x) = & \delta\phi(x) \int_{\Omega_y} \mathcal{B}(x, y) \delta\phi(y) ((I(y) - u_x)^2 - (I(y) - v_x)^2) dy \\ & + \lambda \delta\phi(x) \operatorname{div} \left(\frac{\nabla \phi(x)}{|\nabla \phi(x)|} \right).\end{aligned}\quad (14)$$

The uniform modeling flow finds its minimum energy when the interior and exterior are best approximated by means u and v . In the localized version, the minimum is obtained when each point on the curve has moved such that the local interior and exterior about every point along the curve is best approximated by local means u_x and v_x .

2.2.2 Mean Separation (MS) Energy

Another important global region-based energy that uses mean intensities is the one proposed by Yezzi *et al.* [53] referred to here as the *means separation energy*:

$$E_{\text{MS}} = \int_{\Omega_y} (u - v)^2. \quad (15)$$

This energy relies on the assumption that foreground and background regions should have maximally separate mean intensities. Optimizing the energy causes the curve to move so that interior and exterior means have the largest difference possible. There is no restriction on how well the regions are modeled by u and v . A corresponding F is formed by localizing the global energy with local mean equivalents as shown here:

$$F_{\text{MS}} = (u_x - v_x)^2. \quad (16)$$

By substituting the derivative of F_{MS} into Equation (6) the following local region-based flow is obtained:

$$\begin{aligned}\frac{\partial \phi}{\partial t}(x) = & \delta\phi(x) \int_{\Omega_y} \mathcal{B}(x, y) \delta\phi(y) \cdot \left(\frac{(I(y) - u_x)^2}{A_u} - \frac{(I(y) - v_x)^2}{A_v} \right) dy \\ & + \lambda \delta\phi(x) \operatorname{div} \left(\frac{\nabla \phi(x)}{|\nabla \phi(x)|} \right).\end{aligned}\quad (17)$$

where A_u and A_v are the areas of the local interior and local exterior regions respectively given by

$$A_u = \int_{\Omega_y} \mathcal{B}(x, y) \cdot \mathcal{H}\phi(y) dy \quad (18)$$

$$A_v = \int_{\Omega_y} \mathcal{B}(x, y) \cdot (1 - \mathcal{H}\phi(y)) dy. \quad (19)$$

The optimum of this energy is obtained when u_x and v_x are the most different at every x along the contour. In some cases, this is more desirable than attempting to fit a constant model. Here, local foreground and background means are encouraged to be different rather than constant. This allows this energy to find image edges very well without being distracted when interior or exterior regions are not uniform.

2.2.3 Histogram Separation (HS) Energy

Next, a more complex energy is considered that looks past simple means and compares the full histograms of the foreground and background. Its incorporation into the framework is also straightforward. Consider $P_u(z)$ and $P_v(z)$ to be two smoothed intensity histograms computed from the global interior and exterior regions of a partitioned image I using z intensity bins.

The Bhattacharyya coefficient, \mathfrak{B} , [4] is a measure used to compare probability density functions, and results in a scalar corresponding to the similarity of the two histograms. Recently, Michailovich *et al.* [27] proposed an image segmentation energy,

$$E_{\text{HS}} = \mathfrak{B} = \int_z \sqrt{P_u(z)P_v(z)} dz \quad (20)$$

based on minimizing this measure. This will be referred to as the *histogram separation energy*. It works by separating intensity histograms of the regions inside and outside of the curve, and thus allows interior and exterior regions to be heterogeneous as long as their intensity profiles are different.

In the localized case, $P_{u,x}(z)$ and $P_{v,x}(z)$ will represent the intensity histograms in the local image regions $\mathcal{B}(x, y) \cdot \mathcal{H}\phi(y)$ and $\mathcal{B}(x, y) \cdot (1 - \mathcal{H}\phi(y))$, respectively. As

before the internal energy measure F_{HS} is formed by substituting the local equivalents for $P_u(z)$ and $P_v(z)$ yielding the following expression:

$$F_{\text{HS}} = \int_z \sqrt{P_{u,x}(z)P_{v,x}(z)} dz. \quad (21)$$

By substituting the first variation of F_{HS} into Equation (6) the evolution equation for the localized version of this flow is obtained:

$$\begin{aligned} \frac{\partial \phi}{\partial t}(x) &= \delta\phi(x) \int_{\Omega_y} \frac{\mathcal{B}(x, y)\delta\phi(y)}{2} \left[F_{\text{HS}} \left(\frac{1}{A_v} - \frac{1}{A_u} \right) + \right. \\ &\quad \left. \int_z K(z - I(y)) \left(\frac{1}{A_u} \sqrt{\frac{P_{v,x}(z)}{P_{u,x}(z)}} - \frac{1}{A_v} \sqrt{\frac{P_{u,x}(z)}{P_{v,x}(z)}} \right) dz \right] dy \\ &\quad + \lambda \delta\phi(x) \operatorname{div} \left(\frac{\nabla\phi(x)}{|\nabla\phi(x)|} \right), \end{aligned} \quad (22)$$

where K is a Gaussian kernel.

By using the Bhattacharyya measure to quantify the separation of intensity histograms, the global version of this flow is capable of segmenting objects which have non-uniform intensities. However, the intensity profile of the entire object and the entire background must still be separable. In the localized version, this global constraint is removed but remain capable of effectively separating locally non-homogeneous regions. An example of when this property is useful is shown in the next section.

2.3 Localized Segmentation Results

In Section 2.2 three global energies are presented and localized using the framework described in this work. The experiments below demonstrate the improvements that are offered by such a localization. As with all segmentation techniques, the three global techniques behave somewhat differently from one another. This is due to differences in the underlying assumptions about the given image inherent in each energy. Likewise there are differences in the behavior of the corresponding localized energies. The purpose of the experiments given below is to demonstrate that localization can improve the performance of a given global energy, not to specifically compare the

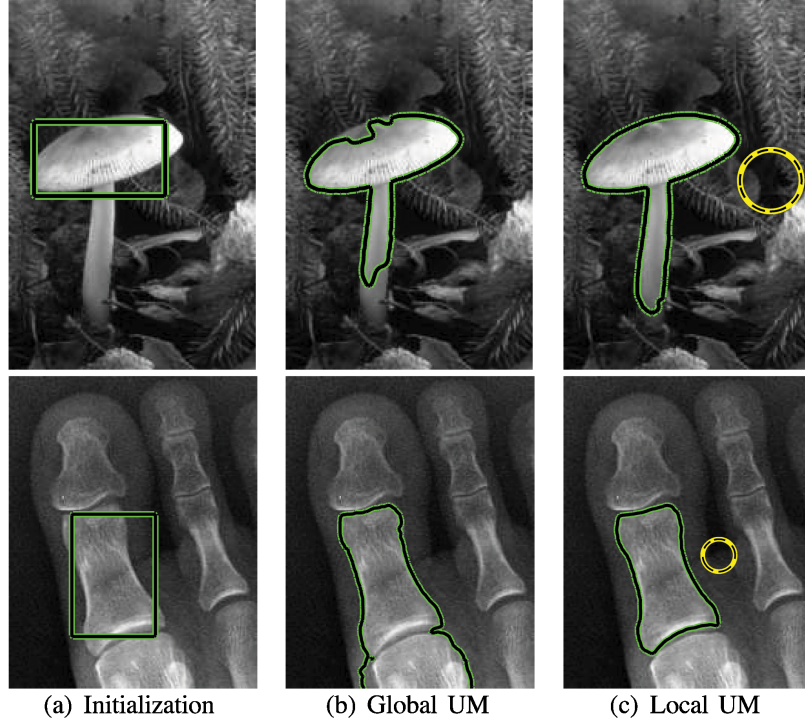


Figure 3: Segmentations of the MUSHROOM and X-RAY image using global and local uniform modeling energy. The dashed yellow circle in (c) represents the localization scale. Localization gives a considerable improvement.

original global energies themselves. In each case, the global energies find segmentations that are consistent with their underlying assumptions about image content but are ultimately incorrect. Only the localized methods are capable of obtaining a correct segmentation in these cases.

Initially, the uniform modeling energy from Section 2.2.1 is considered. In Figure 3, the localized active contour is capable of extending further to find true object boundaries in the MUSHROOM image, and is capable of stopping earlier on true object boundaries in the X-RAY image. These examples show how even images which appear simple can cause significant problems for global techniques. The slight intensity inhomogeneities present in these images prevent global region based methods from correctly capturing the objects.

In Figure 4, the global means separation energy from Section 2.2.2 and its corresponding localization are compared. Notice that the global energy finds only the

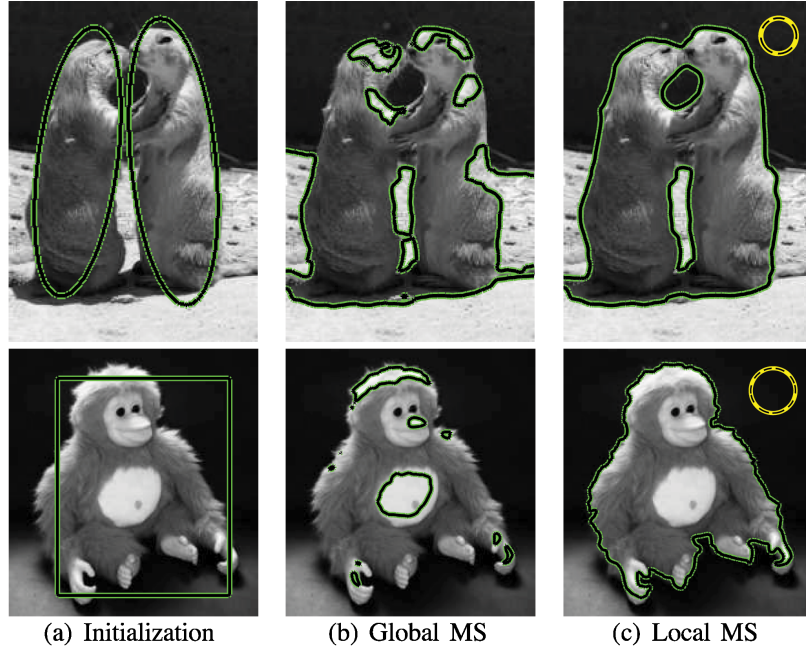


Figure 4: Segmentations of the HUG and MONKEY image using global and local means separation energy. The dashed yellow circle in (c) represents the localization scale. We can see a considerable improvement due to localization.

brightest parts of the image while the localization comes to rest on object boundaries. Both the HUG image and the MONKEY image show objects and backgrounds which are multi-modal, but that have intensities that change smoothly and quickly. In the HUG image in Figure 4, the proposed method is initialized with two ellipses that correspond to a single level set. The contour changes topology as the two ellipses merge to capture both animals. The initial position of the contour (chosen to be between the two animals) is necessary in order for it to segment these holes. Because the level set is only updated in the regions specified by $\delta\phi(x)$, it is not possible for new contours to emerge into this area.

Finally, Figure 5 compares the global histogram separation energy from Section 2.2.3 to its localization. Again, a clear improvement is shown. While the localized contour does not capture the area between the player’s legs, the segmentation found over the rest of the player is much more accurate than in the global case. The PLAYER image shows sharp changes in intensities within the foreground. Strong edges

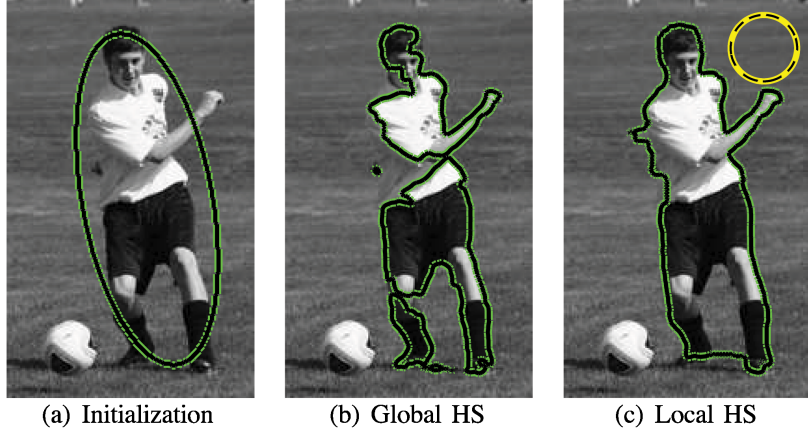


Figure 5: Segmentations of the PLAYER image using global and local histogram separation energy. The dashed yellow circle in (c) represents the localization scale. A considerable improvement is achieved due to localization.

such as those change between the player’s shirt and pants, and between the player’s socks and legs, make the localized histogram separation energy a good choice for this image. Here, the foreground is sometimes locally multi-modal meaning that energies based on local means would have trouble segmenting the image.

For consistency in these experiments, $\lambda = 0.15$ in all trials to weight the influence of contour smoothness. The size of the local radius is shown by the dashed yellow circle drawn on the results for the localized methods. For results involving the global or localized histogram separation energy, 256 bins were used when computing histograms. All segmentations were allowed to run until convergence.

2.4 Fiber Bundle Segmentation

The first medical application for localized active contours considered was the segmentation of neural fiber bundles in diffusion-weighted magnetic resonance images (DW-MRI). These structures have been studied since DW-MRI technology was developed. This imaging modality determines the direction and magnitude of water diffusion at each point in a volume. Because water diffusion is constrained to move along the tube-like axons of neurons in the brain, DW-MRI is useful for analyzing the

connectivity of neurons. As such, a great deal of research has been devoted to finding and characterizing neural connections between parts of the brain using DW-MRI. The resolution of this imagery is typically high enough that major white matter tracts, or bundles of densely packed axons, are several voxels in cross-sectional diameter [29]. The ability to identify the sizes, shapes, and locations of these white-matter tracts is relatively new, but it is gaining momentum as doctors and anatomists begin to understand the physiological significance of this information.

Existing methods that use a global comparison of features tend to do a poor job of segmenting these fiber bundles because of the curving nature of the structures. Alternatively, the approach from Section 2.1 can be used to sample statistics locally and is suited to naturally capture these structures. Once initialized with a single fiber path in the bundle, the proposed method can evolve an active surface driven by local statistics to capture the entire bundle as a single region.

2.4.1 Background and Relevance

Early tractography methods focused on finding single fibers and were based on a technique called *streamlines* which employed local decision-making based on the principal eigenvector of diffusion tensors created from the DW-MRI data [28, 47, 3, 10]. Streamline techniques have been replaced by energy-minimization techniques that use fast marching to find optimal paths based on the same tensor information[37, 35, 22]. More recently, Pichon *et al.* and Melonakos *et al.* use the Finsler metric to find optimal connections based directly on the DW-MRI data data [38, 39, 26, 25]. These optimal paths represents the best connection between the two regions under the given metric. The assumption is that this represents the path of a single fiber.

2.4.1.1 Fiber Bundle Segmentation

As methods to extract single fibers have evolved, surface evolution approaches have been developed in the literature which aim to find the volumetric representation

of the entire bundle of fibers. Rousson *et al.* [44] use a multi-variate Gaussian distribution of the tensor components in a geodesic active region model to drive a surface evolution towards the segmentation of fiber bundles. The method is applied to the segmentation of the corpus callosum, but is unable to fully capture its curved character. Jonasson *et al.* proposed two different ways to address the segmentation of curved fiber bundles in a surface evolution setting: (i) a local approach [15], where the surface evolution speed is influenced by the similarity of a tensor in comparison to its interior neighbors, and (ii) a region-based approach, where the similarity measure is based on the notion of a most representative tensor within the segmented region [16]. In the latter case, capturing highly curved fiber bundles will be problematic because similarity is based on a single representative tensor. The approach proposed here is similar to the work of [15] in as much as it uses local tensor similarities to drive the segmentation. However, Jonasson *et al.* use only a few adjacent pixels to determine local statistics. Using localized statistics as proposed in Section 2.1 allows larger regions of pixels both inside and outside the evolving surface to compete and make the technique more robust to noise and initialization.

2.4.1.2 *The Cingulum Bundle*

In this preliminary work, one major fiber bundle, the cingulum bundle, has been studied. The cingulum bundle is a 5-7 mm in diameter, and interconnects all parts of the limbic system. It originates within the white matter of the temporal pole, and runs posterior and superior into the parietal lobe, then turns, forming a ring-like belt around the corpus callosum, into the frontal lobe, terminating anterior and inferior to the genu of the corpus callosum in the orbital-frontal cortex [45]. The cingulum bundle is crucial in connecting many parts of the brain. It consists of long, association fibers that directly connect temporal and frontal lobes, as well as shorter fibers radiating into their own gyri. The cingulum bundle also includes most afferent

and efferent cortical connections of cingulate cortex, including those of prefrontal, parietal and temporal areas, and the thalamostriatae bundle. In addition, lesion studies of the cingulum bundle document a variety of neurobehavioral deficits resulting from a lesion located in this area, including akinetic mutism, apathy, transient motor aphasia, emotional disturbances, attentional deficits, motor activation, and memory deficits. Also, because of its involvement in executive control and emotional processing, the cingulum bundle has been investigated in several clinical populations, including depression and schizophrenia [19, 50]. The importance of this structure, and the difficulty in segmenting it accurately make it a good choice for study with the proposed technique.

2.4.2 Localized Statistics on Tensor Data

In the case of the cingulum bundle which curves strongly, the tensors across the bundle vary in orientation along the entire length, as shown in Figure 6. In this sagittal view, we see that it is difficult to define a feature on the space of tensors which uniquely separates the entire interior of the cingulum bundle from the exterior. However, we also notice that the tensor shape and anisotropy vary smoothly across the bundle. Hence, locally along the fiber one can define tensor features which are distinguishable from the exterior. In Figure 7 we illustrate this by examining the tensors globally as

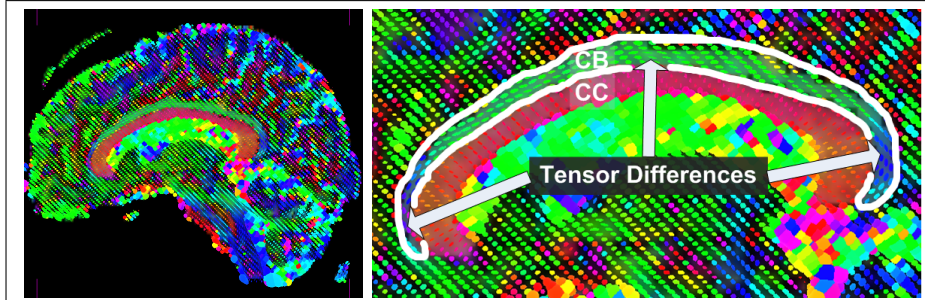


Figure 6: Example of the need for local constraints on region-based segmentation algorithms which attempt to segment the cingulum bundle. Notice how the tensors vary across the length of the cingulum bundle.

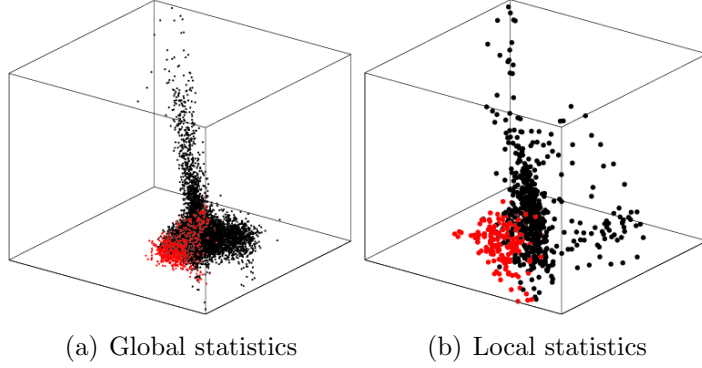


Figure 7: A visualization of the high-dimensional tensors in 3D by projection onto a unit vector. Tensors from the interior of the segmented fiber bundle are shown in *red*, and tensors from the exterior are shown in *black*. (a) Globally, interior and exterior tensors are well mixed and not easily separable. (b) When a local region centered on a point on the surface of the fiber bundle is examined, clusters of interior and exterior tensors appear separable.

well as within a particular local region. Notice how examining local statistics causes more clustering of data from interior and exterior regions respectively.

Let \mathbf{T} denote the volume of directional tensors computed from the DW-MRI data that have been normalized such that $\forall x \|\mathbf{T}(x)\| = 1$. Tensor data consists of six values which represent 3×3 symmetric, positive definite matrix at each voxel. Tensors do not lie in a linear vector space, but instead lie on a conical manifold. Often times analysis of tensor data requires the mapping of tensors to a linear vector space using techniques such as the log-Euclidean mapping [2]. Because of the local nature of the proposed analysis, local regions are still easily separable even when the data is treated as vector-valued volumetric data with the six unique elements of the tensor comprising the value at each voxel. A 3D variation of the energy presented in Section 2.2.1 is used with two slight modifications. First, $\mathbf{u}(x)$ and $\mathbf{v}(x)$ represent the vector-valued interior and exterior means respectively:

$$\mathbf{u}(x) = \frac{\int_{\Omega_y} \mathcal{B}(x, y) \cdot \mathcal{H}\phi(y) \cdot \mathbf{T}(y) dy}{\int_{\Omega_y} \mathcal{B}(x, y) \cdot \mathcal{H}\phi(y) dy} \quad (23)$$

$$\mathbf{v}(x) = \frac{\int_{\Omega_y} \mathcal{B}(x, y) \cdot (1 - \mathcal{H}\phi(y)) \cdot \mathbf{T}(y) dy}{\int_{\Omega_y} \mathcal{B}(x, y) \cdot (1 - \mathcal{H}\phi(y)) dy}. \quad (24)$$

Secondly, the Uniform Modeling energy is modified to simply sum the vector valued components at each voxel:

$$\begin{aligned} E = & \mathcal{H}\phi(y) \left(\sum \mathbf{T}(y) - \mathbf{u}(x) \right)^2 + (1 - \mathcal{H}\phi(y)) \left(\sum \mathbf{T}(y) - \mathbf{v}(x) \right)^2 \\ & + \lambda \int_{\Omega_x} \delta\phi(x) \|\nabla\phi(x)\| dx. \end{aligned} \quad (25)$$

2.4.3 Experiments on Cingulum Bundle Segmentation

The segmentation is initialized with an anchor tract, representing the lowest cost path connecting two maximally spaced-out, pre-defined regions of interest on the fiber bundle to be segmented (the cingulum bundle). This anchor tract is computed using the technique described in [25], but any similar tractography method could be substituted. The result is a single-pixel anchor tract that is then dilated using a $5\text{mm} \times 5\text{mm} \times 5\text{mm}$ ball-shaped structuring element. This produces an initial surface in approximately the correct location. This surface is then deformed in order to minimize Equation (25) and segment the cingulum bundle.

The major parameter used is the localization radius r that describes the formation of the localized statistics which drive the segmentation. This parameter was chosen based on anatomical knowledge that the diameter size of a tensor bundle is at most 7mm [45]. Hence, we used $r = 7\text{mm}$ to ensure that the entire bundle was included in statistical computations. The other parameter used is the weighting coefficient, λ in Equation (25). This parameter controls the intrinsic smoothness of the surface and is set to $\lambda = 0.001$ because the surface is necessarily high in curvature due to its fine structure.

Figure 8 shows the segmentation of the left cingulum bundle as well as the left and right cingulum bundles together. The initialization consists of a single fiber, and is shown as a thin white volume. The final segmentations are shown as thicker yellow volumes. Two views of the final segmentations are provided. Using the proposed

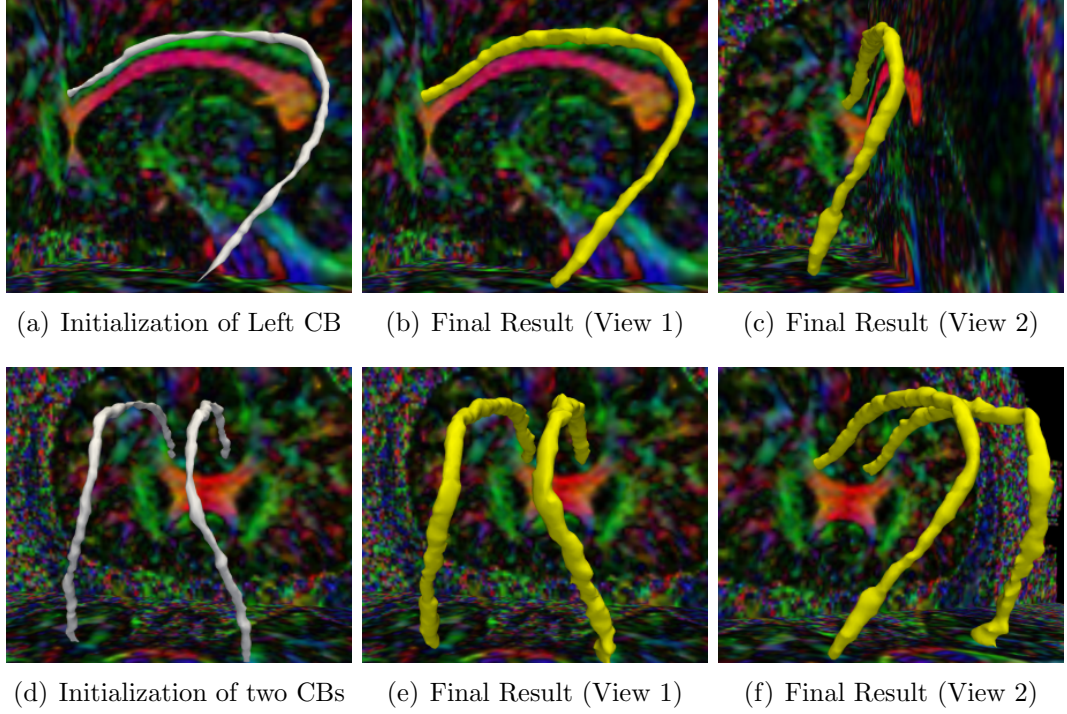


Figure 8: Top Row: Segmentation of left cingulum bundle (CB). (a) Shows initialization from single anchor tract. (b,c) Show multiple views of the final segmentation. Bottom Row: Segmentation of left and right cingulum bundles (CBs) together. (d) Initialization from single tracts. (e,f) Multiple views of the final segmentation.

method, the bundle is segmented without leaking, and captures the changing properties of the bundle as it bends around the corpus callosum. This is all accomplished without any explicit shape prior to defend against leaks. Furthermore, the smoothness of the detected tensor is ensured by the intrinsic properties of the evolving active surface.

CHAPTER III

THE PROPOSED RESEARCH

The object of the proposed research is to explore and improve the use of localized image statistics for image segmentation and consider potential applications to medical image processing. Specifically, the research will include the development of the theory behind the localized framework presented in Chapter 2 and the successful application of this method to fiber bundle segmentation and detection of soft plaque in coronary vessels. Continuation of this research will have three main steps. The first step will be to continue development of the theory and implementation of localization. The second step will focus on the application of these improvements to neural fiber bundle segmentation, soft plaque detection. This will allow the preliminary results to be improved and made more robust to image noise, pathologies, and user input. The third and final step will be to validate these methods and prepare publications that introduce the work to the community. This work is expected to be completed by August 2009.

3.1 Summary of Work Completed

The preliminary work includes the creation of a natural framework that allows any region-based segmentation energy to be re-formulated in a local way. By considering local image statistics and evolving a contour based on local information, the proposed methods are capable of segmenting objects with heterogeneous feature profiles that would be difficult to capture correctly using existing global methods. The presented technique is versatile enough to be used with any global region-based active contour energy and instill in it the benefits of localization. So far, three well-known energies have been localized and studied. Finally, one application, the segmentation of neural

fiber bundles, has been performed with good preliminary results. Other applications have been briefly considered that will be developed and finalized in the remaining research.

3.2 Work Remaining to Be Done

The work remaining will follow the three steps mentioned above. In this section, each step is discussed in greater detail and a timetable for its completion is given. This time-line will be the basis of the work to be completed prior to the dissertation.

3.2.1 Development of Theory and Implementation

The localized framework presented in Section 2.1 provides the basis for the proposed segmentation method. In order to fully explore its abilities, three specific improvements will be researched, developed, and implemented. It is expected that all of these improvements will be completed by the end of April 2009.

3.2.1.1 Weighted Localization Function

The first improvement is the use of a weighting function for local pixels. Currently, the characteristic function, $\mathcal{B}(x, y)$ from Equation (3) is a binary function and classifies pixels as either local or not local. The proposed improvement will be to incorporate a radially symmetric weighting function (such as the Gaussian) to weight closer pixels more than pixels that are far away. This weighting is expected to make the segmentations more robust by providing a more specific concept of locality.

3.2.1.2 Coupled Contours

The second improvement will be the coupling of two or more contours each driven by localized energies. Allowing multiple contours to interact dynamically will allow multiple objects to be segmented simultaneously. Early indications are that coupling localized active contours will be instrumental in detecting soft plaque in coronary vessels. The method for coupling the contours will be based on the work of Brox *et*

al. [7], but will be expanded to apply more specifically to the local-looking nature of the proposed segmentation technique.

3.2.1.3 Optimized Implementation

Finally, the current implementations of the proposed local methods run rather slowly. In order to improve the usability of this method, the codes will be re-implemented with an eye towards optimization. This should reduce the time that it takes segmentations to complete.

3.2.2 Additional Applications

With the completion of the improvements mentioned above, the preliminary results on the cingulum bundle from Section 2.4.3 should be able to be improved somewhat, and new applications will become possible as well. This step is projected to be completed in May 2009.

3.2.2.1 Continuation of Fiber Bundle Segmentation

The addition of kernel weighting while performing localization will likely improve the preliminary segmentation results on the cingulum bundle and allow other neural fiber bundles to be segmented more easily. With these enhanced capabilities, segmentation will be attempted on the corpus callosum and additional datasets containing the cingulum bundle. Performing these test will help show the robustness of the technique.

3.2.2.2 Detection of Soft Plaque

One new application will involve the study of arteriosclerosis. There has recently been an interest in using CTA imagery to study of coronary vessels [12, 46, 30]. Some recent work has been done in segmenting vessels and detecting plaques in this imagery, [41, 51]. Early experimentation suggests that localized active contours may be useful for detecting harmful *soft plaques* within these vessels that existing techniques can not detect well. Using two coupled active contours to simultaneously detect the interior

and exterior of the vessel wall, it is expected that soft plaques can be identified by finding places of increased wall thickness. A specific protocol for using localized active contours to detect plaques in this way will be developed and tested.

3.2.3 Validation and Preparation of Publications

Once these improvements have been made and tested, they will be checked by medical professionals that can collaborate to determine if the results have improved to the point where they can be useful to the medical community. These doctors will assist by identifying results as “correct” or “incorrect” as well as providing feedback on how the results can be improved. This qualitative evaluation is necessary due to the lack of solid ground-truth data available. These final validations will then be used in creating and submitting publications so that this research can reach a wide audience. There are two expected journal submissions. The first will finish the preliminary work on neural fiber bundle segmentation, and the second will describe a method for soft plaque detection. The work to create and submit these publications will also double as work towards the writing a full thesis. This work will begin in May and finish in July of 2009 in anticipation of a defense in August 2009.

3.3 Facilities Needed

Due to the nature of this work, the facilities required are very minimal. The needed resources include access to a computer work-station, a high-performance computing cluster for some experiments, and licenses for Mathworks MATLAB. These resources have already been acquired, and are currently available. Additionally, relationships with doctors capable of providing data, validating results and providing insight into the applicability of the research will be needed. These relationships have already been formed. Doctors at Emory University Hospital in Atlanta have agreed to collaborate on the study of coronary vessels, and doctors at Brigham and Women’s Hospital in Boston will assist in validating neural fiber bundle analysis.

APPENDIX A

DERIVATION OF CURVATURE FLOW

Recall the first term from the original definition of E in terms of a generic internal energy F in Equation (5):

$$E(\phi) = \int_{\Omega_x} \delta\phi(x) \int_{\Omega_y} \mathcal{B}(x, y) F(I(y), \phi(y)) dy dx. \quad (26)$$

To compute the first variation of this term, a change of parameters is performed to express $E(\phi)$ as $E(\phi + \xi\nu)$:

$$E(\phi + \xi\nu) = \int_{\Omega_x} \delta(\phi(x) + \xi\nu) \int_{\Omega_y} \mathcal{B}(x, y) F(I(y), \phi(y) + \xi\nu) dy dx. \quad (27)$$

Here, ν represents a small perturbation along the normal direction of ϕ weighted by a scalar ξ .

Next, the partial derivative of this energy is taken with respect to ξ evaluated at $\xi = 0$ to represent a tiny differential of movement. By the product rule,

$$\begin{aligned} \nabla_\xi \Big|_{\xi=0} E &= \int_{\Omega_x} \delta(\phi(x)) \int_{\Omega_y} \nu \mathcal{B}(x, y) \nabla_{\phi(y)} F(I(y), \phi(y)) dy dx + \\ &\quad \nu \int_{\Omega_x} \gamma\phi(x) \int_{\Omega_y} \mathcal{B}(x, y) \cdot F(I(y), \phi(y)) dy dx \end{aligned} \quad (28)$$

is obtained. Note that $\gamma\phi$ denotes the derivative of $\delta\phi$. On the zero level set $\gamma\phi$ evaluates to zero. As such, it does not affect the movement of the curve and thus this term is ignored. Now the integral over y is moved outside the integral over x :

$$\nabla_\xi \Big|_{\xi=0} E = \int_{\Omega_y} \int_{\Omega_x} \nu \delta(\phi(x)) \mathcal{B}(x, y) \nabla_{\phi(y)} F(I(y), \phi(y)) dx dy. \quad (29)$$

At this point, the Cauchy-Schwartz inequality is used to show that the optimal direction to move ϕ is given by:

$$\frac{\partial\phi}{\partial t} = \int_{\Omega_y} \delta(\phi(x)) \mathcal{B}(x, y) \nabla_{\phi(y)} F(I(y), \phi(y)) dx dy. \quad (30)$$

Re-arranging the integrals once more gives the same equation in a form that is easier to understand. This yields the final curve evolution

$$\frac{\partial \phi}{\partial t} = \delta\phi(x) \int_{\Omega_y} \mathcal{B}(x, y) \cdot \nabla_{\phi(y)} F(I(y), \phi(y)) dy \ dx. \quad (31)$$

REFERENCES

- [1] AN, J., ROUSSON, M., and XU, C., “ γ -convergence approximation to piecewise smooth medical image segmentation,” in *Proc. Med. Imag. Comput. Comp. Assist. Interven.*, vol. 4792, pp. 495–502, 2007.
- [2] ARSIGNY, V., FILLARD, P., PENNÉC, X., and AYACHE, N., “Log-euclidean metrics for fast and simple calculus on diffusion tensors,” *Magnetic Resonance in Medicine*, vol. 56, pp. 411–421, 2006.
- [3] BASSER, P., PAJEVIC, S., PIERPAOLI, C., DUDA, J., and ALDROUBI, A., “In vivo fiber tractography using DT-MRI data,” *Magnetic Resonance in Medicine*, vol. 44, no. 4, pp. 625–632, 2000.
- [4] BHATTACHARYYA, A., “On a measure of divergence between two statistical populations dened by their probability distributions,” *Bull. Calcutta Math. Soc.*, vol. 35, pp. 99–110, 1943.
- [5] BLAKE, A. and ISARD, M., *Active Contours*. Cambridge: Springer, 1998.
- [6] BROX, T. and CREMERS, D., “On the statistical interpretation of the piecewise smooth mumford-shah functional,” in *Proc. Scale Space and Var. Met. in Comp. Vis.*, vol. 4485, pp. 203–213, 2007.
- [7] BROX, T. and WEICKERT, J., “Level set segmentation with multiple regions,” *IEEE Trans. Image Process.*, vol. 15, pp. 3213–3218, October 2006.
- [8] CASELLES, V., KIMMEL, R., and SAPIRO, G., “Geodesic active contours,” *Int. J. Comput. Vis.*, vol. 22, pp. 61–79, Feb. 1997.
- [9] CHAN, T. and VESE, L., “Active contours without edges,” *IEEE Trans. Image Process.*, vol. 10, pp. 266–277, Feb. 2001.
- [10] CONTURO, T., LORI, N., CULL, T., AKBUDAK, E., SNYDER, A., SHIMONY, J., MCKINSTRY, R., BURTON, H., and RAICHLE, M., “Tracking neuronal fiber pathways in the living human brain,” *Proc Natl Acad Sci US A*, vol. 96, no. 18, pp. 10422–10427, 1999.
- [11] CREMERS, D., ROUSSON, M., and DERICHE, R., “A review of statistical approaches to level set segmentation: Integrating color, texture, motion, and shape,” *Int. J. of Comp. Vis.*, vol. 72, no. 2, pp. 195–215, 2007.
- [12] DEHMESHKI, J., YE, X., AMIN, H., ABAEI, M., LIN, X. Y., and QANADLI, S., “Volumetric quantification of atherosclerotic plaque in ct considering partial volume effect,” *IEEE Transactions on Medical Imaging*, vol. 26, no. 3, pp. 273–282, 2007.

- [13] GONZALEZ, R. and WOODS, R., *Digital Image Processing*. Prentice Hall, 2001.
- [14] HORN, B., *Robot Vision*. MIT Press, 1986.
- [15] JONASSON, L., BRESSON, X., HAGMANN, P., CUISENAIRE, O., MEULI, R., and THIRAN, J., “White matter fiber tract segmentation in DT-MRI using geometric flows,” *Medical Image Analysis*, vol. 9, no. 3, pp. 223–236, 2005.
- [16] JONASSON, L., HAGMANN, P., POLLO, C., BRESSON, X., WILSON, C., MEULI, R., and THIRAN, J., “A level set method for segmentation of the thalamus and its nuclei in DT-MRI.,” *Signal Processing*, vol. 87, no. 2, pp. 309–321, 2007.
- [17] KICHENASSAMY, S., KUMAR, A., OLVER, P., TANNENBAUM, A., and JR., A. Y., “Conformal curvature flows: From phase transitions to active vision,” *Arch. Ration. Mech. Anal.*, vol. 134, pp. 275–301, Sept. 1996.
- [18] KIM, J., FISHER, J., YEZZI, A., CETIN, M., and WILLSKY, A., “A nonparametric statistical method for image segmentation using information theory and curve evolution,” *IEEE Trans. Image Process.*, vol. 14, pp. 1486–1502, Oct. 2005.
- [19] KUBICKI, M., WESTIN, C., NESTOR, P., WIBLE, C., FRUMIN, M., MAIER, S., KIKINIS, R., JOLESZ, F., MCCARLEY, R., and SHENTON, M., “Cingulate fasciculus integrity disruption in schizophrenia: a magnetic resonance diffusion tensor imaging study,” *Biological Psychiatry*, vol. 54, no. 11, pp. 1171–1180, 2003.
- [20] LANKTON, S. and TANNENBAUM, A., “Localizing region-based active contours,” *Image Processing, IEEE Transactions on*, vol. 17, pp. 1–11, Nov. 2008.
- [21] LANKTON, S., MELONAKOS, J., MALCOLM, J., DAMBREVILLE, S., and TANNENBAUM, A., “Localized statistics for dw-mri fiber bundle segmentation,” in *Wkshp. Math. Meth. Biomed Imag. Anal.*, Jun 2008.
- [22] LENGLET, C., ROUSSON, M., DERICHE, R., FAUGERAS, O., LEHERICY, S., and UGURBIL, K., “A Riemannian Approach to Diffusion Tensor Images Segmentation,” *Proceedings of the 19th International Conference on Information Processing in Medical Imaging (IPMI), Glenwood Springs, CO, USA*, pp. 591–602, 2005.
- [23] LI, C., KAO, C.-Y., GORE, J., and DING, Z., “Minimization of region-scalable fitting energy for image segmentation,” *Image Processing, IEEE Transactions on*, vol. 17, pp. 1940–1949, Oct. 2008.
- [24] LI, C., KAO, C.-Y., GORE, J. C., and DING, Z., “Implicit active contours driven by local binary fitting energy,” in *Proc. Comput. Vis. Pattern Recog.*, June 2007.

- [25] MELONAKOS, J., MOHAN, V., NIETHAMMER, M., SMITH, K., KUBICKI, M., and TANNENBAUM, A., “Finsler tractography for white matter connectivity analysis of the cingulum bundle,” *MICCAI*, 2007. to appear.
- [26] MELONAKOS, J., PICHON, E., ANGENENT, S., and TANNENBAUM, A., “Finsler active contours,” *IEEE Transactions on Pattern Analysis and Machine Intelligence*, 2007. in press.
- [27] MICHAILOVICH, O., RATHI, Y., and TANNENBAUM, A., “Image segmentation using active contours driven by the bhattacharyya gradient flow,” *IEEE Trans. Image Process.*, vol. 15, pp. 2787–2801, November 2007.
- [28] MORI, S., CRAIN, B., CHACKO, V., and VAN ZIJL, P., “Three-dimensional tracking of axonal projections in the brain by magnetic resonance imaging.,” *Ann Neurol*, vol. 45, no. 2, pp. 265–9, 1999.
- [29] MORI, S. and VAN ZIJL, P., “Fiber tracking: principles and strategies- a technical review,” *NMR in Biomedicine*, vol. 15, no. 7-8, pp. 468–480, 2002.
- [30] MOTOYAMA, S., KONDO, T., SARAI, M., SUGIURA, A., HARIGAYA, H., SATO, T., INOUE, K., OKUMURA, M., ISHII, J., ANNO, H., VIRMANI, R., OZAKI, Y., HISHIDA, H., and NARULA, J., “Multislice computed tomographic characteristics of coronary lesions in acute coronary syndromes,” *Journal of the American College of Cardiology*, vol. 50, no. 4, pp. 319–326, 2007.
- [31] MUMFORD, D. and SHAH, J., “Optimal approximations by piecewise smooth functions and associated variational problems,” *Comm. Pure Appl. Math*, vol. 42, pp. 577–685, 1989.
- [32] MUMFORD, D., “A bayesian rationale for energy functionals,” in *Geometry Driven Diffusion in Computer Vision* (ROMENY, B., ed.), Kluwer Academic, Dordrecht, pp. 141–153, 1994.
- [33] OSHER, S. and FEDKIW, R., *Level Set Methods and Dynamic Implicit Surfaces*. New York, NY: Cambridge University Press, 2003.
- [34] OSHER, S. and TSAI, R., “Level set methods and their applications in image science,” *Commun. Math. Sci.*, vol. 1, no. 4, pp. 1–20, 2003.
- [35] ODONNELL, L., HAKER, S., and WESTIN, C., “New Approaches to Estimation of White Matter Connectivity in Diffusion Tensor MRI: Elliptic PDEs and Geodesics in a Tensor-Warped Space,” *Computing and Computer Assisted Intervention (LNCS)*, vol. 2488, pp. 459–466, 2002.
- [36] PARAGIOS, N. and DERICHE, R., “Geodesic active regions: A new framework to deal with frame partition problems in computer vision,” *Int. J. Comput. Vis.*, vol. 46, pp. 223–247, Feb. 2002.

- [37] PARKER, G., WHEELER-KINGSHOTT, C., and BARKER, G., “Estimating distributed anatomical connectivity using fast marchingmethods and diffusion tensor imaging,” *Medical Imaging, IEEE Transactions on*, vol. 21, no. 5, pp. 505–512, 2002.
- [38] PICHON, E., *Novel methods for multidimensional image segmentation*. PhD thesis, Georgia Institute of Technology, 2005.
- [39] PICHON, E., WESTIN, C., and TANNENBAUM, A., “A Hamilton-Jacobi-Bellman approach to high angular resolution diffusion tractography,” *Eighth International Conference on Medical Image Computing and Computer-Assisted Intervention (MICCAI05). Lecture Notes in Computer Science*, vol. 3749, pp. 180–187, 2005.
- [40] PIOVANO, J., ROUSSON, M., and PAPADOPOULO, T., “Efficient segmentation of piecewise smooth images,” in *Proc. Scale Space and Var. Met. in Comp. Vis.*, vol. 4485, pp. 709–720, 2007.
- [41] RENARD, F. and YANG, Y., “Coronary artery extraction and analysis for detection of soft plaques in mdct images,” in *IEEE International Conference on Image Processing*, pp. 2248–2251, Oct. 2008.
- [42] ROUSSON, M. and DERICHE, R., “A variational framework for active and adaptive segmentation of vector valued images,” in *Wkshp. Motion Vid. Computi.*, p. 56, 2002.
- [43] ROUSSON, M., LENGLET, C., and DERICHE, R., “Level set and region based propagation for diffusion tensor MRI segmentation,” in *Wkshp. Math. Meth. Biomed Imag. Anal.*, pp. 123–134, 2004.
- [44] ROUSSON, M., LENGLET, C., and DERICHE, R., “Level Set and Region Based Surface Propagation for Diffusion Tensor MRI Segmentation,” *Computer Vision and Mathematical Methods in Medical and Biomedical Image Analysis*, vol. 3, no. 5, p. 36, 2004.
- [45] SCHMAHMANN, J. and PANDYA, D., *Fiber Pathways of the Brain*. Oxford University Press, 2006.
- [46] SCHROEDER, S., KOPP, A., and BURGSTAHLER, C., “Noninvasive plaque imaging using multislice detector spiral computed tomography,” *Seminars in Thrombosis and Hemostasis*, vol. 33, no. 2, pp. 203–209, 2007.
- [47] STIELTJES, B., KAUFMANN, W., VAN ZIJL, P., FREDERICKSEN, K., PEARLSON, G., SOLAIYAPPAN, M., and MORI, S., “Diffusion Tensor Imaging and Axonal Tracking in the Human Brainstem,” *NeuroImage*, vol. 14, no. 3, pp. 723–735, 2001.

- [48] SUM, K. and CHEUNG, P., “A novel active contour model using local and global statistics for vessel extraction,” in *Proc. Eng. Medicine Bio. Soc.*, pp. 3126–3129, 2006.
- [49] SUM, K. and CHEUNG, P., “Vessel extraction under non-uniform illumination: A level set approach,” *IEEE Trans. on Biomed. Eng.*, vol. 55, pp. 358–360, Jan. 2008.
- [50] WANG, F., SUN, Z., CUI, L., DU, X., WANG, X., ZHANG, H., CONG, Z., HONG, N., and ZHANG, D., “Anterior Cingulum Abnormalities in Male Patients With Schizophrenia Determined Through Diffusion Tensor Imaging,” 2004.
- [51] YANG, Y., *Image segmentation and shape analysis of blood vessels with applications to coronary atherosclerosis*. PhD thesis, Georgia Institute of Technology, 2007.
- [52] YEZZI, A., TSAI, A., and WILLSKY, A., “A statistical approach to snakes for bimodal and trimodal imagery,” in *Proc. Int. Conf. Comput. Vis.*, vol. 2, pp. 898–903, 1999.
- [53] YEZZI, A., TSAI, A., and WILLSKY, A., “A fully global approach to image segmentation via coupled curve evolution equations,” *J. Vis. Comm. Image Rep.*, vol. 13, pp. 195–216, Mar. 2002.
- [54] ZHU, S. C. and YUILLE, A., “Region competition: Unifying snakes, region growing, and bayes/mdl for multiband image segmentation,” *IEEE Trans. Pattern Anal. Mach. Intell.*, vol. 18, pp. 884–900, Sept. 1996.